JCTC Journal of Chemical Theory and Computation

Multiscale Modeling of the Atomic Layer Deposition of HfO_2 Thin Film Grown on Silicon: How to Deal with a Kinetic Monte Carlo Procedure

A. Dkhissi,* A. Estève, C. Mastail, S. Olivier, G. Mazaleyrat, L. Jeloaica, and M. Djafari Rouhani

Laboratoire d'Analyse et d'Architecture des Systèmes-CNRS, University of Toulouse, 7 avenue du Colonel Roche, 31077 Toulouse, France

Received April 09, 2008

Abstract: An original integrated approach developed within a multiscale strategy, which combines first-principles quantum simulations and kinetic Monte Carlo (KMC), is presented to investigate the atomic layer deposition (ALD) of HfO_2 on Si(100) surface. Density functional theory within the hybrid functional is used to determine the detailed physicochemical mechanisms and associated energetics of the two half cycles taking place during the initial stage of film growth. A kinetic Monte Carlo model is then proposed that deals with the stochastic nature of the calculated DFT mechanisms and barriers. Beyond the chemical information emanating from DFT calculations, the lattice-based KMC approach requires preliminary physical considerations issued from the crystal structures that the system is intended to adopt. This is especially critical in the case of heterogeneous systems like oxides deposited on silicon. We also describe (i) how atomistic configuration changes are performed as a result of local events consisting in elementary reaction mechanisms occurring on specific lattice sites, (ii) the temporal dynamics, governed by transition probabilities, calculated for every event from DFT activation barriers, and (iii) the relation of KMC with the ALD experimental procedure. Some preliminary validation results of the whole multiscale strategy are given for illustration and pertinence with regard of the technological main issues.

Downloaded via LEIBNIZ UNIVERSITAET HANNOVER on December 6, 2024 at 13:06:23 (UTC).
See https://pubs.acs.org/sharingguidelines for options on how to legitimately share published articles.

1. Introduction

In the electronic field, SiO_2 has been the gate dielectric of choice for MOS devices for several decades because of its ability to grow on silicon, its thermal stability, and its low level of defect density at the interface, resulting in excellent electrical properties of the devices. Unfortunately, the reduction of the SiO_2 gate oxide thickness in agreement with Moore's law has led to unacceptable tunnelling and leakage current levels.[1] So, the conventional SiO_2 gate reaches its physical and electrical limitations. An intense effort to find a replacement for SiO_2 as the gate dielectric for future MOS electronics has been under way for several years. For this purpose, the importance of high-*k* gate dielectrics has been well demonstrated.[2] Indeed, in addition to showing a high dielectric constant, a potential high-*k* replacement must satisfy many stringent requirements, such as the high quality of the interface, a desired band alignment with silicon, and a large electronic gap. At present, the leading materials are Al_2O_3, HfO_2, and ZrO_2 oxides, considered as the first high-*k* generation candidates to meet these criteria and replace SiO_2. For MOS applications, HfO_2 is attractive because it exhibits a bulk permittivity of almost 25, a wide band gap (5.68 eV), and a good thermodynamic stability in contact with silicon.[3] However, the growth of a SiO_2 interfacial layer between HfO_2 and the silicon substrate leads to an increase of the experimental EOT (equivalent oxide thickness) of the gate stack.

Among various methods for growing high-*k* dielectric films, atomic layer deposition (ALD) show a unique ability to deposit ultra thin films with excellent conformity and uniformity over large areas.[4] ALD, which is a vapor

* To whom correspondence should be addressed. E-mail: adkissi@laas.fr.

10.1021/ct8001249 CCC: $40.75 © 2008 American Chemical Society
Published on Web 10/15/2008

deposition technique, is based on the cycling of self-terminating surface reactions. Indeed, each precursor is pulsed into the reaction chamber alternately, and the reaction between the incoming precursors and surface species is self-terminating. Thus atomic-level control of film growth is supposed to be achieved. Experimentally, ALD has been actively investigated for deposition of HfO_2[5−21] for which $HfCl_4$ and H_2O are often used as precursors.[22−24] In practice, the quantity of metal atoms deposited per cycle depends on the temperature, on the chemical nature of the precursors used, and related reactive sites on the surface. For instance, Ritala et al. found that only a submonolayer of the HfO_2 film is deposited during each cycle.[22] Therefore, a detailed understanding of the basic mechanisms that take place during each cycle is required if one wants to optimize the deposition and to reach full monolayer coverage at each cycle. This is especially true for the few first deposited layers whose quality, in terms of interface defects, is of major importance for subsequent electrical properties. In recent studies, some groups have investigated specific problems of ALD of hafnia films, their structural, optical, and electrical characteristics.[25−28] They show that diffusion and solid-state reactions at the substrate−film interface may influence the film material and create or modify an interface layer between the film and substrate.[29] On silicon substrates, these reactions could result in undesirable formation of defects, silicate or silicide layers, which may further significantly deteriorate the properties of the dielectric layer.[29−32] Others issues, such as contamination effects resulting from the uncontrolled precursor decomposition, are observed. In particular, chlorine contamination has been asserted and well documented on films grown with $HfCl_4$ precursors.[20,33−35] It is of great importance for optimal future experimental setups that a precise atomic level description of the basic reaction mechanisms responsible for the overall process of high-*k* film growth and also that their relation with the thermodynamic parameters be established. In this respect, the decomposition of $HfCl_4$ on the substrate and further hydrolysis of the resulting surface complex, that is, SiO_2−O−$HfCl_3$ should be thoroughly investigated. Meanwhile, today's state-of-the-art theoretical methods can play a decisive role in reduction of the expensive experimental efforts needed for screening large numbers of candidate materials and associated process parameters. Theoretical approaches can speed up the selection of suitable gate dielectrics and growth methods by limiting the experimental input needed. For these reasons, a detailed understanding of the basic mechanisms that take place during each cycle of ALD has been the subject of intensive research effort by several theoretical groups using first principles, especially via density functional theory.[35−51] In our group, we have considered the ab initio study of the initial stage of the ALD as being essential for the complete understanding and the control of the growth of the high-*k* (Al_2O_3, ZrO_2, and HfO_2) films for gate dielectrics applications.[49−51] Our final aim is to achieve the ambitious task of elaborating a new generation of tools dedicated to atomic scale simulation of technological process, for an optimization of experimental setups. Here, our strategy is to combine the ab initio level of calculations with kinetic Monte-Carlo techniques into a multiscale approach, which will incorporate enough reaction mechanisms to be ready for being tested against experimental setups. Rigorously, molecular dynamics should be a suitable tool to address atomic scale process simulation. However, microelectronic processes deal with mesoscopic structures, several millions of atoms, and cover timescales beyond seconds or minutes. Molecular dynamics is then limited for two major reasons: (i) interatomic potentials have to be generated, which is a particularly difficult task in the frame of heterostructures and interfaces, and (ii) timescales are limited to nanoseconds of experimental duration. Thus kinetic Monte Carlo (KMC) is an alternative procedure that is of great help in the modeling of microelectronic processes: a lattice-based model makes it possible to avoid the detailed description of continuous atomic trajectories, and the kinetics of the sequence of events is explicitly treated and can meet typical process durations. While traditional thermodynamic and kinetic models deal with average physical quantities, kinetic Monte Carlo is able to consider a wide range of possible configurations at the atomic scale and to choose only one random path out of all possible ones. This corresponds to an actual (ALD) experiment. The path is determined according to random numbers sampled according to transition probabilities between configurations. Obviously, the transition probabilities depend also on the local configuration, activation barriers and on the film deposition conditions, such as pressure and temperature. Moreover the role of each mechanistic step on an ensemble of interacting species makes it feasible to uncover process-dependent types of growth, kinetics, and their associated atomic arrangements. The present paper is dedicated to the description of the preliminary version of our KMC tool enabling the treatment of HfO_2 ALD from $HfCl_4$ and H_2O precursors at the atomic scale. In the following, we will focus our attention on the basic ingredients needed to develop what we call a lattice-based KMC model. We will define a lattice framework able to represent the transition from the silicon diamond structure to the HfO_2 crystalline structure. Then we introduce the concept of basic atomistic mechanisms and show how they can be derived from ab initio calculations. We will finally present the temporal dynamics rules of our model before showing validation and applications.

2. Theoretical Approaches

2.1. Ab Initio DFT. The calculations are performed within the framework of Kohn−Sham density functional theory. Specifically, we used the hybrid functional B3-LYP, which combines Becke's three-parameter exchange functional (B3)[52] with Lee−Yang−Parr gradient corrected correlation functional (LYP).[53] All the atoms are described by a triple-ζ valence plus polarization (TZVP) functions. For Hf atoms, we used the ecp-60-mwb energy-consistent pseudopotentials given by the Stuttgart−Dresden−Bonn (SDB) group.[54−56]

The surface is built according to the following procedure. It is modeled by a cluster that includes a dimer unit of the 2×1 reconstructed Si(100) surface having each of its Si dangling bonds passivated by an H atom. Only the first Si

layer atoms are left free during the relaxation. The second-, third-, and fourth-layer atoms, including the H terminations, are held fixed in their bulk tetrahedral positions. This type of constraint will avoid unrealistic relaxations of the surface model during the optimization procedure. The unconstrained part of the cluster was then oxidized by five oxygen atoms placed in the Si−Si bonds closest to the surface. Therefore, subsequent relaxations were performed after each newly arrived O atom was embedded. The result is 1-dimer peroxide-like[57,58] model for $Si(100)/SiO_2$ 2×1 surface. Of the two remaining dangling bonds on the dimer, one is hydroxylated and the other hydrogenated. One then obtains a 28-atom optimized structure with a final stoichiometry of $Si_9O_6H_{13}$. The calculations are performed with Turbomole5.5[59] and Gaussian03.[60]

2.2. Kinetic Monte Carlo (KMC). KMC is a stochastic-based model aimed at simulation of film growth at the atomic scale, the final objective being to furnish alternative/new tools for replacement of the macroscopic conventional TCAD tools used for years by engineers in microelectronics. Indeed, from the engineering point of view, the main interest is in the microstructure that is produced under specific processing conditions. Such a model performs virtually the explicit experimental processing procedure event after event, at the atomic scale. This is operated through probabilistic rules that make the overall simulation comparable with an actual experiment.[61,62] It involves millions of atoms with a time duration longer than the second. Unfortunately, the most predictive models, that is, the quantum-based models are not tractable at this scale. Two options can be further considered: molecular dynamics (MD) and kinetic Monte Carlo (KMC). MD solves the Newton equation of motion for each atom in the system. Trajectories are continuous and necessitate very short integration time steps that make the simulation cumbersome for durations beyond the nanosecond. Another drawback of the MD method is the general lack of adequate interatomic potential for highly disordered and heterogeneous systems. This is particularly true for microelectronics semiconductor/oxide interfaces such as silicon/high-*k* gate oxides. KMC appears to be a simplification compared with MD: MD continuous trajectories are replaced with discrete atomic jumps. A prior knowledge of these hoppings is needed and must be listed from any other source: quantum-based models or experimental characterization. Thus, provided the characteristics of reaction pathways are known, KMC methods allow the simulation of more ambitious systems in terms of size and duration of the simulated experiment, meeting the requirements of the next generation of processes in microelectronics. Also, the lattice-based KMC, because of its induced structural simplification, makes it easier to process the data concerning the atomic arrangement as a function of the implemented basic mechanisms. This contrasts with the difficulty in dealing with structural aspects in MD, where complex statistical methods have to be employed.

Basic ingredients needed to develop what we call a lattice-based KMC model are detailed as follows: (i) we first define a lattice framework able to operate the desired transition between the silicon crystal and the oxide structure; (ii) we then characterize each configuration with the aim of associating each lattice site to the chemical nature of the species occupying the site; (iii) we introduce the concept of events that must describe correctly the chemistry of the basic mechanisms; (iv) we finally indicate how to deal with the time evolution in the KMC, namely, the temporal dynamics of the KMC.

2.2.1. One Crystal Lattice Model. 2.2.1.1. Lattice Description. In contrast to molecular dynamics, where atoms are moving continuously in space, the lattice-based procedure developed in this KMC software allows a very efficient treatment of atomic displacements: the atoms discretely move from predefined sites to other sites according to transition probabilities. Obviously, this schematic picture is motivated by physicochemical considerations through the knowledge of the basic mechanisms and the investigation of lattice structure. This last point becomes crucial in the case of heterogeneous systems, where at least two different crystallographic structures are being considered. This is the case in our study, where metallic oxides are grown on an ultrathin silicon oxide, itself grown or deposited on a silicon substrate. First, a reliable and systematic way of representing the atom locations is needed. Then, the implementation of configurations makes the connection between a location and its chemical nature: for instance, a site may be unoccupied or occupied by Si, Hf, etc.We point out that this lattice picture gives the possibility of making schematic and comprehensive graphical views of the system and therefore of performing a simple analysis of the results that does not require complex post-processing of the data. In this description, where an atom is represented in its network site, its real location is implicitly somewhere around this particular site.

2.1.1.2. Modeling of the Atomic Configuration. We now describe the construction of a model in charge of representing the atomic configuration of a $Si/SiO_2/HfO_2$ system of sites. Beyond the crystalline aspects, we will introduce tools able to take into account the molecular states: precursors, substituents, contaminants, etc. The management of the neighbors will also be investigated. Attention will finally be given to the modeling of the substrate and its connection with the introduced crystalline model. Overall crystallinity is defined when Hf and oxygen atoms are located in the predefine lattice sites. In this case, Hf may be fully or under-coordinated depending on the occupancy of the oxygen lattice sites around. When densification occurs, rearrangement of oxygen atoms should induce an increase of the coordination number.

a. Crystallographic Considerations. A preliminary crystallographic study is essential in close connection with the construction of the atomic configuration. In our case, the system is heterogeneous: "high-*k*" oxide on silicon with an ultrathin silica interface. Moreover, the basic species are molecular precursors whose mechanisms of decomposition prove to be complex and poorly understood. It is thus necessary to develop a system of location able to represent simultaneously various crystalline structures containing various elements. Moreover, further refinements will be necessary to take account of several subtleties, such as molecular states, substituents, and contaminants, in opposition to crystalline states. First of all, it is advisable to know the crystallography of the HfO_2 oxide. Hafnia exists under

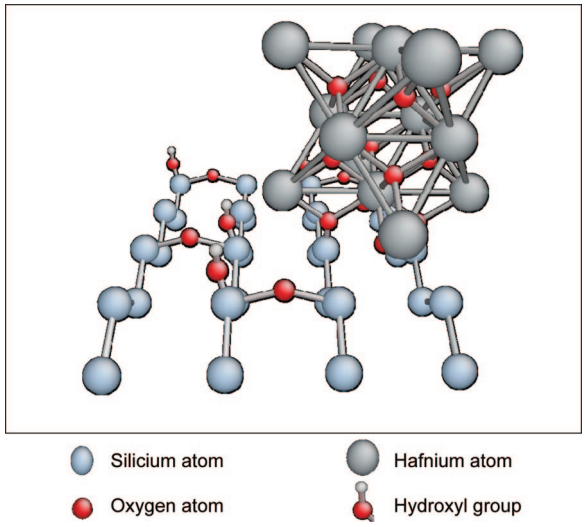

Figure 1. Cubic cell of hafnia deposited on the Si/SiO_2 substrate functionalized with hydroxyl groups.

different crystallographic structures. At low temperature, HfO_2 has a monoclinic phase. When the temperature is increased, it transforms into the tetragonal phase and then into the cubic phase. Experimental evidence of crystalline grains for thick oxide or post-annealed films has been established. However, the structure close to interface, that is, the oxide structure near the silicon/silicon dioxide, is not known. Therefore, to correctly model this interface, one has to make a coincidence lattice site study. For us, it then appears judicious to consider the (100) face of the cubic phase of hafnia: it matches efficiently the (100) silicon surface structure, is geometrically easier to describe, and does not contradict or hinder the experimental results. Thus, the overall idea consists of building the model of location via a single cubic structure, keeping in mind that the real positions of atoms are "somewhere around" these arbitrary crystalline positions. The substrate will be a Si(100) surface functionalized by hydroxyl groups, which are known to be the active surface sites with regard to the precursor gas phase. [63]

b. Two-Dimensional Basic Cell. To characterize the sites in our KMC, we have to define a two-dimensional cell where there should not be any ambiguity between atom species and locations. For that, we superimpose the conventional cubic cell of oxide and silicon-based SiO_2 (100) surface and try to find an agreement between their crystallographic parameters. The silicon surface structure is taken as the crystal reference, an ultrathin silicon dioxide being able, in this view, to accommodate perfectly with this structure. We obtain the hypothetical configuration represented in Figure 1. This resulting picture leads to the best agreement between the different cells. The silicon substrate is represented by two atomic layers to know the orientation of the bonds in the higher layers. In Figure 1, siloxane bridges and hydroxyl functions are represented just as an indication. This surface representation is very schematic: in particular, we do not show the dimer formation inducing Si−O−Si species, although they are taken into account in the calculations. Silicon atoms are schematically located at the nodes of the diamond lattice, without taking account of displacements usually observed. According to the crystallographic tables,[64]

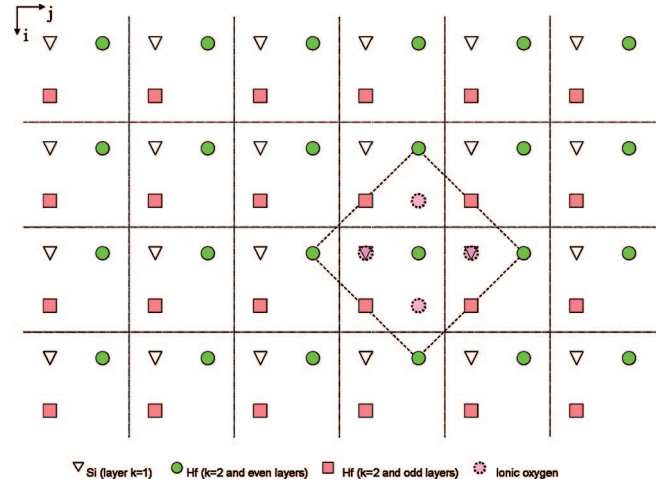

Figure 2. Top view of ideal configuration. Several HfO_2 cubes are deposited on the substrate with an ideal agreement of cell. A two-dimensional cell is identified where there should not be any ambiguity between atom species and locations.

the distance separating two Si surface atoms is 3.84 Å. If one then considers that the cubic cell parameter of hafnia oxide is 5.04 Å, the distance separating two neighboring Hf atom is 3.57 Å. It thus appears possible to accommodate the two structures, thanks to the coincidence between Si(100) and Hf(100), with a tension of the cubic hafnia that can be assimilated to an intrinsic strain at the interface level of the. In more detail, how do Hf positions compare to those of Si? The answer that we formulated is illustrated in Figure 1.

Let us imagine now that we deposit several HfO_2 cubes in tension, as seen previously, on the substrate, with an ideal agreement of the cells. We see that a tilt of the cell is required to obtain a complete matching of the atoms. It is then possible to completely cover the surface without defect. It is, to some extent, what we would like to obtain in real experiments, the defects resulting from the kinetic process and the stochastic nature of the growth. Figure 2 is a top view of this ideal configuration where the various species are represented by symbols for a better legibility. We thus have a (100) surface of silicon atoms, covered by single-crystal HfO_2 in its cubic phase. The square base of a conventional cubic cell is represented in dotted line. Five hafnium atoms are located in the second layer ($k = 2$): the four corners of the square and the central atom (gray round symbols). On the monolayer above ($k = 3$), we find four hafnium atoms corresponding to the centers of the four side faces (gray square symbols). The first four oxygen atoms (gray round symbols on dotted line) are situated between these two layers ($k = 2 + {}^1/_2$). By addition of two new layers, one of oxygen atoms (gray round symbols on the dotted line at $k = 3 + {}^1/_2$) and one of hafnium atoms (gray round symbols at $k = 4$), one obtains the totality of the conventional cube. This cube is obviously not the primitive cell, minimal for the construction of a crystal. The primitive cell, which we consider to be the unit cell, is represented in thick dotted lines and is found by observation of Figure 2 globally. According to altitude, or more exactly to the layer index k, one meets various species, placed at various positions of this cell. For the $k = 1$ layer, we have a silicon placed on a

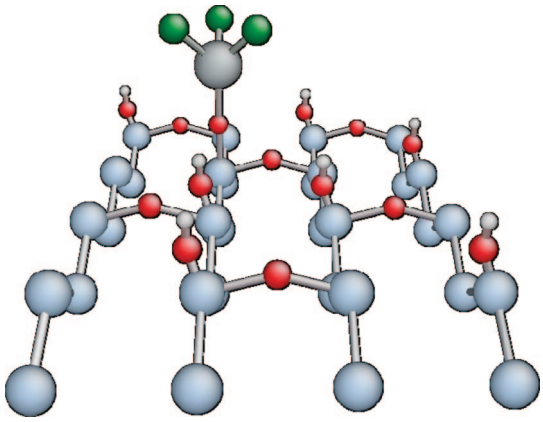

Figure 3. Noncrystalline −O−$HfCl_3$ groups chemisorbed on the hydroxylated Si/SiO_2. This is the KMC model structure

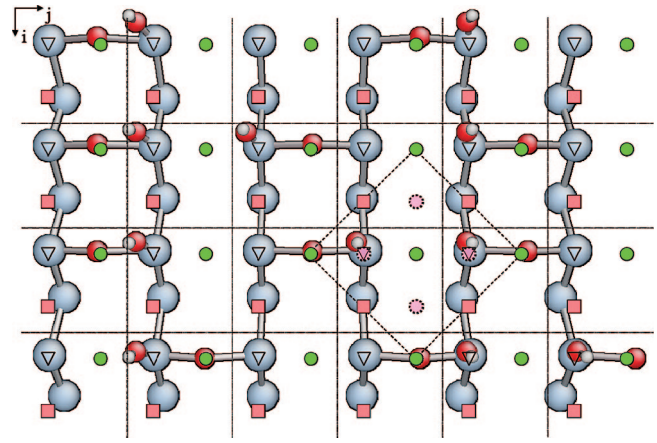

Figure 4. Connection between the atomic model of configuration and the substrate.

triangle. For the even layers, a hafnium will be placed on a gray round symbol, and for the odd layers (except $k = 1$), hafnium will be located on a dark gray square. Between two layers of hafnium, we find two oxygen atoms placed on the gray round dotted lines (for clarity, they are represented only in the conventional cell). This primitive cell thus makes it possible to represent in an exhaustive way an HfO_2 crystal, in its cubic phase, on a (100) silicon surface. It contains preset sites that are able to accommodate the various atoms that compose the system, while placing them at the adequate position.

c. Atomic Configurations. Through the lattice description, we built a grid to help us to locate the atoms. Now we must formalize the possible chemical nature of species occupying these sites. Thus, the configuration, that is, the site occupation nature, should characterize the local atomic arrangement within the site. We introduce a data-processing structure that will take account not only the crystalline configuration but also the chemical functions, the various contaminants, and the molecular groupings with their substituent. Each element of grid will thus contain several fields of occupation. For the metal element, it is provided in molecular form in the precursor, is then incorporated as an adsorbed molecule, and finally, is stabilized in the crystalline state. Therefore, the field of metal occupation can be empty (value 0), be occupied by a molecular hafnium (value 1), or occupied by a crystalline hafnium (value 2). A crystalline state corresponds to the case where a hafnium is located somewhere around a preset site, while being based on the cubic cell of dense oxide. On the other hand, in its molecular state, the Hf atom is attached to the substrate by only one connection, that is, a treelike structure, after physisorption or chemisorption of the precursor molecule. It is advisable to distinguish these two states because their reactivities will be, without any doubt, different because one Hf−OH or Hf−Cl dangling bond transforms into Hf−O−Si−substrate (Sub) tightly bound to the substrate. As an example, Figure 3 presents one such molecule, a chemically absorbed grouping, having three Cl substituents attached. The substituents have their own fields of occupation: one for Cl and one for OH. The values of these two fields can reach 4; their sum has to remain lower than 4 to respect the coordination number of hafnium atoms in their covalent environment. For the crystalline oxygen atoms considered in the construction of the elementary cell, two fields of O_a and O_b sites are identified. They can be empty or occupied. Let us recall that these oxygen atoms are of crystalline type and do not have to be confused with those of hydroxyls or the groupings, O−Hf, which are considered as molecular.

These oxygen crystalline sites can be occupied after what we will call "densification" mechanisms, described later in Section 3.1.3.The reaction mechanisms presented in the following section predict a possible contamination by HCl, a byproduct issued from precursor chemisorption. This led us to introduce a field of occupation HCl to account for its presence near a hafnium center, crystalline or not. By convention, for the hydrolysis phase, adsorbed water will be represented by the value 3 in the metal field of occupation. Each element of our table of atomic configuration will thus be a structure containing several fields of occupation (metal, Cl, OH, O_a, O_b, HCl) and being able to take various values. This occupancy table will play a major role during the execution of the software: in permanent evolution, it will be questioned and in turn modified very frequently until the final configuration is obtained. The use of grid indices, preset sites within a basic cell and fields of occupation will allow a faithful representation of the system, while guaranteeing a light and fast data-processing, authorizing an exploration on a mesoscopic scale.

d. Neighborhood. To determine, in an efficient way, if a chemical reaction is possible or not within the crystal, it is necessary to know the state of occupation of neighboring cells in the grid. Therefore, it is very important to know precisely the neighbors of a given site. We define 12 neighbors per lattice site, taking periodic boundary conditions into account.

e. Substrate Modeling. Figure 4 shows connection between the atomic model of network based configuration and a hydroxylated Si/SiO_2 (100) substrate, by the superposition of the chart of the system and the symbols of the network based model (Si−H are not represented). It is seen here that the silicon atoms take the places that are reserved for them (triangles) with internal displacements, in particular, on the level of dimers, being neglected. Siloxanes and hydroxyls are distributed according to options described previously. One notes that preset sites are empty, "on standby" for the arrival

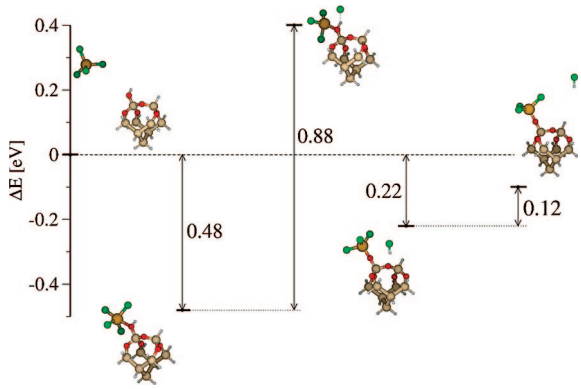

Figure 5. Initial reaction path way and associated barriers in the case of HfCl4 based precursor ALD on SiO_2/Si.

of a hafnium or an oxygen. These crystalline positions will be occupied through molecular transient states, as considered in the fields of occupation of the table of configurations.

2.2.1.3. Mechanisms and Events. To avoid confusion, we need to define what we mean by "reaction step" and by KMC "event". A reaction step is an elementary or single chemical reaction. An event is related to the Monte Carlo procedure; it stands for a mechanism that occurs at a particular time on a well-determined site within the grid.

a. Mechanism Definition. The elementary reaction steps that constitutes the basis of any KMC approach can emanate from literature data, ab initio calculations, or a KMC investigation itself (in particular cases where the code is ready for validation procedures). As an example, Figure 5 illustrates precursor chemisorption, followed by HCl desorption. The calculated activation energies, using ab initio DFT, can serve as preliminary input values for the kinetic Monte Carlo mechanisms. The results of ab initio calculations are summarized in Section 3.1. Further, ALD growth is complicated by other reaction steps, not just the precursor molecule's adsorption and hydrolysis. An example is the densification (Table 1). Indeed, a key technological question that arises during the film growth is the necessary phase transition of the interesting materials from their molecular structure in the gas-phase precursors to their solid-state structure in the deposited film. This is particularly true for metallic compounds, such as oxides (HfO_2), where the metal has a covalent bonding structure in the precursor, with a small coordination number, while the metal oxides have mainly ionic structures with large coordination numbers. However, the complexity of the densification process is such that our present KMC implementation includes no changes in Hf or O coordination number. Further, because of the intrinsic difficulty in consideration of reaction steps related to these phenomena, the set up of a DFT modeling strategy becomes tricky. Later on in the paper, densification will be clarified, and we will show how this problem can be overcome in the KMC.

b. Events Filtering and Modified Probability Sites. Let us begin with an example, the precursor arrival mechanism. Obviously, there are lots of precursor arrival events, onto every surface site. But, at a given time, not all these events are possible. They must be filtered, or in other words, authorized or forbidden. The authorized events list is updated

Table 1. List of Mechanisms Considered in the KMC Simulations, with Their Main Characteristics, As Described in the Text

DFT investigation	KMC investigation[a]
01 HfCl4 adsorption	09 Dens. Inter_Cl_1N_cOH-iOH (all *k*)
02 H2O adsorption	10 Dens. Inter_Cl_1N_cOH-iCl (all *k*)
03 HfCl4 Desorption	11 Dens. Inter_Cl_1N_cCl-iOH (all *k*)
04 HCl incorporation	12 Dens. Inter_Cl_2N_cOH-iOH (all *k* except 2)
05 H2O Desorption	13 Dens. Inter_Cl_2N_cOH-iCl (all *k* except 2)
06 H2O incorporation	14 Dens. Inter_Cl_2N_cCl-iOH (all *k* except 2)
07 back reaction	15 Dens. Intra_Cl_1N_cOH-iOH ($k = 2$)
08 HCl Desorption	16 Dens. Intra_Cl_1N_cOH-iCl ($k = 2$)
	17 Dens. Intra_Cl_1N_cCl-iOH ($k = 2$)
	18 Dens. Intra_CC_1N_cOH-cOH ($k = 2$)
	19 Dens. Intra_CC_1N_cOH-cCl ($k = 2$)
	20 Dens. Intra_CC_2N_cOH-cOH ($k = 2$)
	21 Dens. Intra_CC_2N_cOH-cCl ($k = 2$)
	22 Dens. Bridge_Tl_2N_tOH-iOH ($k = 2$)
	23 Dens. Bridge_Tl_2N_tOH-iCl ($k = 2$)
	24 Dens. Bridge_Tl_2N_tCl-iOH ($k = 2$)
	25 Dens. Bridge_Tl_3N_tOH-iOH ($k = 2$)
	26 Dens. Bridge_Tl_3N_tOH-iCl ($k = 2$)
	27 Dens. Bridge_Tl_3N_tCl-iOH ($k = 2$)
	28 Dens. Bridge_TC_3N_tOH-cOH ($k = 2$)
	29 Dens. Bridge_TC_3N_tOH-cCl ($k = 2$)
	30 Dens. Bridge_TC_3N_tCl-cOH ($k = 2$)
	31 Dens. Bridge_TC_4N_tOH-cOH
	32 Dens. Bridge_TC_4N_tOH-cCl
	33 Dens. Bridge_TC_4N_tCl-cOH
	34 Dens. Bridge_TT_3N_tOH-tOH ($k = 2$)
	35 Dens. Bridge_TT_3N_tOH-tCl ($k = 2$)
	36 Dens. Bridge_TT_4N_tOH-tOH
	37 Dens. Bridge_TT_4N_tOH-tCl
	38 Dens. Bridge_TT_5N_tOH-tOH
	39 Dens. Bridge_TT_5N_tOH-tCl

[a] Densifications may result from reactions between Cl or OH terminals in ionic (i), cluster (c), or tree (t) configurations.

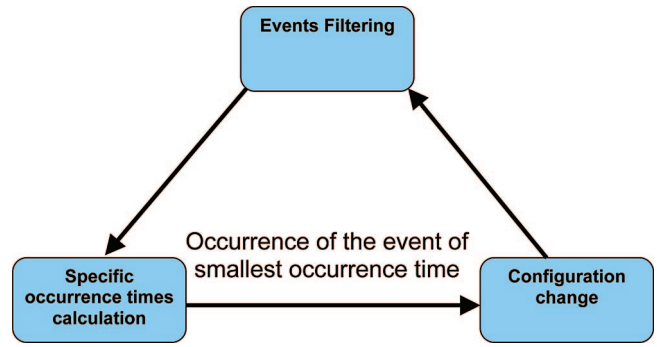

Figure 6. Kinetic Monte Carlo cycle.

at each system configuration change. Moreover, if one given event is forbidden and becomes authorized, its "specific time" is also updated (see Section 2.2.1.2b for details about this point). In contrast, if the event is authorized and remains authorized, its "specific time" is kept as is. In any other case, the forbidden event's "specific time" is set to a value greater than the overall experiment duration. If not reauthorized again, this event will never occur. To save computing time, the filtering procedure is only called when necessary by a "smart call" routine, Figure 6. Another way to save computing time is to consider modified probability sites (MPS). In this procedure, after the occurrence of a given event, one considers only a local reactualization of the sites/events/time of occurrence. Rigorously, all the sites/events could be reactualized, which would require a huge amount of computing time. This procedure is thus used on the basis of the

concept that an event has a limited impact in space and that domains far from the occurring event do not see it.

3. Results and Discussion

3.1. Ab Initio Results. To date, almost all ab initio investigations have focused on the chemistry of possible reactions, during both precursor and water exposures of the ALD of HfO_2. These predictive methods, cluster or periodic based-DFT, are particularly suitable for chemical mechanisms that are difficult to reach by experiment or other modeling strategies.

Here, the reactions between the gaseous precursors $HfCl_4$ or H_2O with the hydroxylated SiO_2 surface are predicted to proceed via an exchange mechanism[65,66] and can be separated into two half reactions. The first half-cycle reaction (1) takes place during the initial step of atomic layer deposition of HfO_2, that is, the decomposition of $HfCl_4$ precursor molecules, followed by a purge

$$||SiO_2-OH + HfCl_4 \rightarrow ||SiO_2-O-HfCl_3 + HCl \quad (1)$$

The second half cycle (2) is exposure to water molecules and is also followed, in practice, by a purge period.

$$||SiO_2-O-Hf(OH)_{3-x}-Cl_x + H_2O \rightarrow SiO_2-O-Hf(OH)_{4-x}-Cl_{x-1} + HCl \quad (2)$$

where x has values of 1−3.

First, we give the results of the first half-cycle reaction at the initial deposition step. The second task is dedicated to the second half reaction. We present results and compare them with those related to ZrO_2. Data from the literature are also discussed. However, the basic mechanisms that are given in the following are crucial to understand the results all along the multiscale procedure up to the KMC/experiment relation. All basic mechanisms have been introduced in the KMC and are activated all along the ALD process duration, except chemisorptions of water and precursor from gas-phase exposure that are limited to specific semicycles. Their desorptions, reactions, and backreactions are possible through all cycles. Their occurrence will depend on the computed activation energies.

3.1.1. Precursor/Surface Reaction: Overview of Existing Results. Geometrical structures and energetic diagram of the total system along the decomposition reaction pathways of $HfCl_4$ on the SiO_2 substrate are presented in Figure 5. A chemisorbed state is found where Hf/O interaction is occurring without substantial modification of the precursor integrity (0.48 eV adsorption energy). This adsorption energy is weaker than those obtained by Musgrave and co-workers.[66] This difference is the result of the differences in cluster geometry and basis set. Both parameters are more extended in our study. A dissociation path is then calculated, and we obtain an activation barrier of 0.88 eV. This barrier is higher than the 0.7 eV barrier obtained by Widjaja et al..[68] The difference is caused by the methodology used in the search of transition state and the surface models that are different. Beyond the saddle point, HCl molecule formation is observed during minimization with subsequent adsorption of this molecule on top of the dimer inserted oxygen atom. Globally, it is expected from these results that the deposition with the desired coverage of a complete monolayer of precursors is a difficult task. The sticking of the precursor is low. The high activation barrier for decomposition is compared to the precursor non dissociative chemisorption. Moreover, the dissociative incorporation is reversible. The dissociated precursor molecule is itself thermodynamically unstable with respect to the chemisorbed state. This authorizes the precursor to recombine and to be rejected from the surface. Fortunately, the HCl byproduct desorption is fast, because of its low activation energy of only 0.12 eV, and inhibits further reverse reaction. These qualitative aspects will be confirmed at the KMC modeling level.

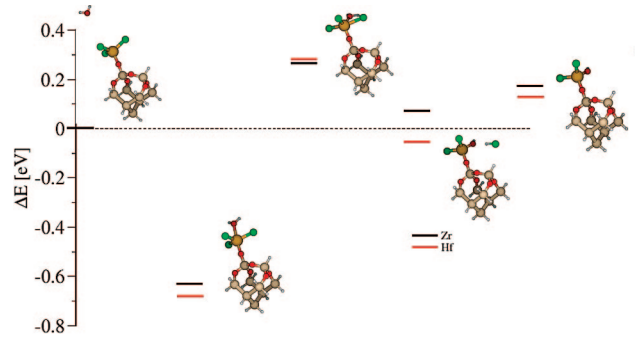

Figure 7. Reaction path and predicted energetics for the reactions of H_2O and $SiO_2-O-HfCl_3$ and H_2O and $SiO_2-O-ZrCl_3$.

3.1.2. Hydrolysis Reaction. The second half cycle, which introduces H_2O into the reaction chamber, is intended to regenerate the surface-OH group by reaction 2. The reaction path and predicted energetic for the reaction of H_2O on $||SiO_2-O-HfCl_3$ sites are presented in Figure 7. For comparison, we also report, in this figure, the results of the reaction of H_2O on $||SiO_2-O-HfCl_3$. The energy levels are displayed relative to initial state energy. Further, Table 2 summarizes the energetic data for the two reactions and compares them with corresponding results obtained by Musgrave and co-workers.[67−69]

The quantitative energetic of the reaction 2, shown in Figure 8, shows some similarities between HfO_2 and ZrO_2. Indeed, water molecule adsorbs onto the $HfCl_3$ (or $ZrCl_3$) covalently bonded to the surface by donating a lone pair from the oxygen atom to the empty d shell of the Hf. In the case of HF (or Zr), the complex chemisorbed state is 0.68 eV (or 0.62 eV) more stable than the initial state. After the adsorption of H_2O, the reaction proceeds via the transition state shown in Figure 8. In the transition state, O in H_2O is bonded to Hf with a bond length of 1.9 Å. The Hf−Cl distance is increased to 3.8 Å, which indicates that the bond is broken in the transition state. We also note that the interaction between the O lone pair and the HCl antibonding orbital leads to the delocalization of the lone pair electrons, which indicates the partial breaking of the O−H bond and the partial formation of HCl bond. The reaction is exothermic by 0.19 eV with an activation barrier of 0.97 eV. As shown in Table 2 and Figure 8, the second half reaction for Zr has the same behavior as for Hf. Indeed, the saddle point energies for the two systems are also close leading to an activation

Table 2. Comparisons of Energetic (In eV) for the Si−O−M(Cl)$_3$+ H_2O (M = Hf, Zr) and Those Obtained from Literature[a]

	M−Cl_3−H_2O complex	TS[b]	M−$OHCl_2$−HCl complex	HCl desorption
M = HF	0.68	0.97	0.63	0.20
M = Zr	0.62	0.90	0.69	0.09
M = Zr (results of Musgrave, ref 68)	0.78	0.88	0.75	0.05

[a] The energies of M−Cl_3−H_2O are relative to the entrance channel. The energies of TS, M−$OHCl_2$−HCl complex are relative to the M−Cl_3−H_2O complex. The energies of HCl desorption are relative to the M−$OHCl_2$−HCl complex. [b] Transition state.

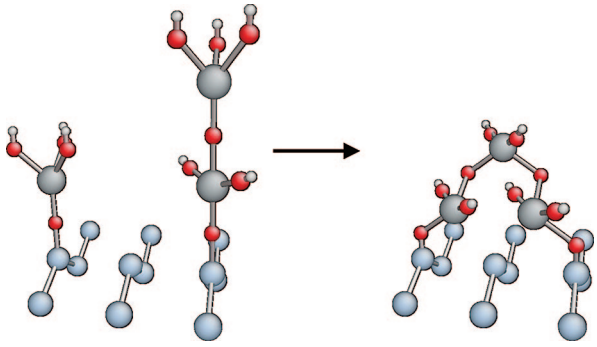

Figure 8. Example of densification mechanism: multilayer noncrystalline/tree.

barrier of 0.97 and 0.90 eV for Hf and Zr, respectively. In comparison with the data obtained by Musgrave et al., the choice of cluster geometry and basis set led to systematic differences in relative energies, except that a similar barrier is obtained by Musgrave (0.88 eV) and us (0.90 eV).

Further, on the basis of the results obtained by Musgrave and us, the use of clusters models should be sufficient to determine the reaction mechanisms. To determine the credibility of DFT in predicting these mechanisms, Heyman et al.[35] reported the calculations (especially transition states) on different precursors using DFT, MP2, and QCISD(T) and concluded that both ab initio approaches resulted in the same transition states that were found using DFT (B3LYP).

3.1.3. Densification Mechanisms. Beyond reaction mechanisms appears a key issue for a better understanding of high-*k* film growth, we will call the phenomenon "densification". In the gas phase, metallic precursors exhibit a covalent molecular structure characterized by a small coordination number, whereas the resulting deposited metallic oxide has an ionic type of structure characterized by a large coordination number. This necessary phase transition has been poorly investigated to date in literature.[50] In our recent work, we show that this chemical process is mediated by the presence of oxygen atoms: sharing them locally allows a local redistribution of oxygen atoms and metallic centers to operate the desired transition. This implies an increase of the coordination of both Hf and oxygen atoms and a "more dense" local reallocation of the atoms through the collapse of dendritic tree like structures into densely packed oxide films. The dendritic structures result from an accumulation of adsorbed molecules, preventing a dense structure by steric hindrance. However, the complexity of the densification process is such that our KMC model still poorly describe this phenomenon leading to no increase of the coordination number.

In addition, we expect new insight from DFT calculations in this area in the future (currently under investigation in our team) because no such reaction pathway has been calculated in the frame of the ALD process specifically.

3.2. Preliminary KMC Results. *3.2.1. Mechanisms in Kinetic Monte Carlo Code.* The kinetic Monte Carlo code contains all the above generic mechanisms, declined in various cases and configurations. These are detailed in Table 1, where we distinguish between two types of mechanisms, respectively listed in the two columns of Table 1. The first column contains eight mechanisms whose thermodynamic and kinetic parameters are calculated using DFT. It contains precursor adsorption, desorption, incorporation and back reaction, H_2O adsorption, desorption and incorporation (hydrolysis), and HCl byproduct desorption.

The second column contains 31 (09−39) mechanisms of densification type whose rates are empirically adjusted by comparison of simulation results with experimental data. These densification mechanisms can occur between precursors situated on the same layer (intra) or different layers (inter). They can also occur in situations where the creation of a bridge, with overhangs left in the growing film, is necessary. On the other hand, densifications can occur between neighboring sites, up to the fifth neighbors. Densifications may also result from reactions between Cl or OH terminals in ionic (i), cluster (c), or tree (t) configurations. These denominations refer respectively to terminals directly adsorbed on the film surface (i), which are therefore in ionic positions, to terminals on precursor molecule deposited on the film surface as a cluster (c), and to terminals on treelike precursor molecules (t). These latter are molecules bonded to an already adsorbed molecule. They allow the adsorption of several layers of precursor molecules on the surface.

All the above information, together with the layer number *k*, where the corresponding events can occur, is reported in Table 1. In addition, in Figure 8, we give an example of densification mechanism.

The energetic of reactions 09−39 are set to one arbitrary value and later fitted to experiment. This will help to bring out the importance of further modeling of these reactions.

3.2.2. Optimization of Substrate Hydroxylation. Hydroxylated surfaces can be prepared using various processes[70,71] that allow preparation of surfaces with different densities of reaction sites. We thus simulate a first ALD phase, at 300 °C, with a duration of 100 ms verusus the 50 ms duration generally used in experiments. We have performed simulations ((10 × 10) atoms substrates) on five different initial substrates containing various OH concentrations. The first four cases concern 25%, 50%, 75%, and 100% hydroxyl concentrations, with siloxane bridges distributed randomly; 100% coverage corresponds to one OH per surface silicon atom. The fifth case concerns the simulation of the hydroxy-

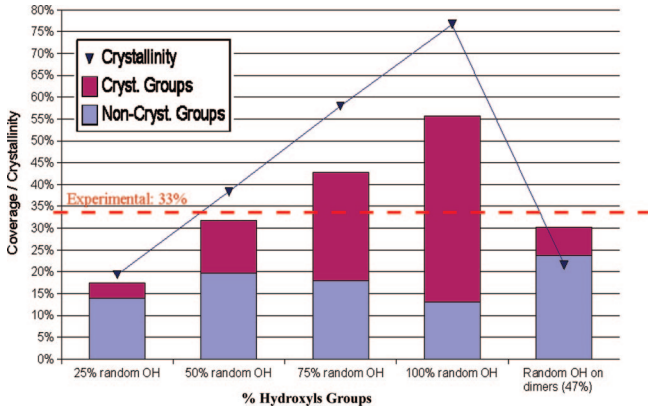

Figure 9. Evolution of coverage rates (HfO_2 coverage) and crystallinity with different initial substrates.

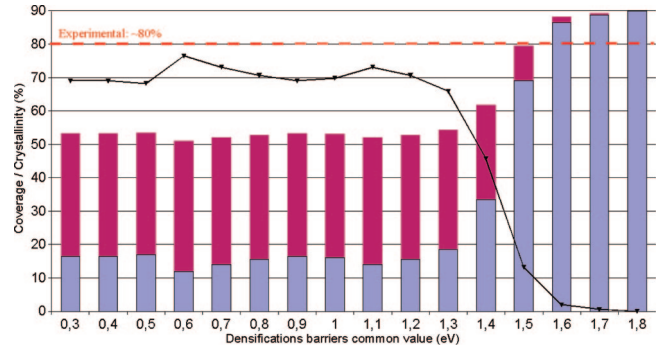

Figure 10. Calibration of energies of the first densifications.

lation process with the option "no more than one OH on each dimer". This process leads to 47% hydroxyl coverage.

The coverage rates (HfO_2 coverage) obtained, after one ALD cycle, are represented on the graph of Figure 9, where we have also distinguished between the crystalline and molecular states of Hf. Again, 100% coverage corresponds to one Hf per surface silicon atom. The triangles in Figure 9 show the crystallinity ratio. An increase in the total coverage is observed when one increases the number of reactive sites on the substrate. Moreover, crystallinity follows the same tendency: this is the result of the possibility for a chemically absorbed precursor to bridge itself if an OH is available in its vicinity. In the case with 100% hydroxyl coverage of the surface, it is noted that the total coverage amounts to approximately 55%, indicating that a majority of hafnium atoms are thus bridged. In this case, each Hf reacts with two OH: one for the sticking and one for the bridging process. The bridging process can be considered as one type of densification mechanism because it allows the elimination of one branch within the molecular tree structure.

We cannot judge yet if this is realistic because the barriers of these first densifications are unknown, and arbitrary values are introduced at this stage. At the end of the first ALD cycle performed at 300 °C on a chemical silicon oxide, a total coverage of 35% has been experimentally measured.[69] This value is in good agreement with our simulations with 50% OH and 47% OH. These concentrations are indeed the most probable ones when referring to the model of Zhuravlev, dealing with the hydroxylation of SiO_2 surfaces.[72] In addition, in the last case, by limiting the local OH concentrations, we hinder the densification mechanisms: crystallinity is 22% in the fifth case, while 38% in the second case with 50% OH.

3.2.3. Calibration of Energies of First Densifications. In practice, densification mechanisms in the kinetic Monte Carlo account for all transitions from molecular state to ionic or crystalline states, that is, the nodes of the lattice. These include reactions between grafted molecular ligands and the surface, such as the bridging process (eq 3) or reactions between two grafted ligands close to each other. The activation energies of all the mechanisms of densification are unknown and not well understood to date.[73] We have arbitrarily fixed them at 0.5 eV for preliminary simulations. Their values have no incidences on the coverage at low hydroxyl concentrations and at the usual growth temperatures. But, if underestimated, the coverage can decrease at high hydroxyl concentrations. In this case, the most probable reaction is between two first neighbors OH, to bridge a single Hf, as expressed in eq (3)

$$\mathrm{Si{-}O{-}HfCl_3 + Si{-}OH \rightarrow Si{-}O{-}HfCl_2{-}O{-}Si + HCl} \quad (3)$$

Actually, in the KMC scheme, the global bridging mechanism is broken in two steps, chemisorption and densification, each one consuming a single OH. If the energy barriers for the first densification are increased, the densification rates decrease, and the most probable configurations will be two separate chemisorptions on two OH groups, without any densification, as in eq 4

$$\mathrm{2Si{-}OH + 2HfCl_4 \rightarrow 2Si{-}O{-}HfCl_3 + 2HCl} \quad (4)$$

The competition between eqs 3 and 4 can be quantified by comparing KMC results with the experimental values of the coverage.[70] From these experiments, we can estimate very roughly that with a surface covered with 90% hydroxyl, one should obtain, after one ALD cycle on a (10 × 10) atom substrates, a HfO_2 coverage of approximately 80%. This is in total disagreement with preceding simulations. We thus launched several simulations of the first precursor injection phase of ALD, performed at 300 °C during 200 ms, while varying the energy barrier for densifications between 0.3 and 1.8 eV. We should mention that in a given simulation, the same value is applied to all the densifications. Figure 10 shows the HfO_2 coverage and crystallinities obtained for these various densification barriers. For weak densification barriers, we observe a strong crystallinity, proof that a majority of Hf atoms are bridged thanks to the great number of hydroxyls. For higher values of densification barriers, chemisorption takes place, leading then to less crystallinity but more extensive coverage. The simulation that approaches 80% of experimental measured coverage is that with a densification barrier of 1.5 eV. This calibration should be, at first sight, very approximate. The experimental criterion translated into atomic terms is not inevitably reliable, and all the densifications may not be equivalent. Despite these naive considerations, the transition seen by variation of the densification energy appears to be abrupt, a few tenths of

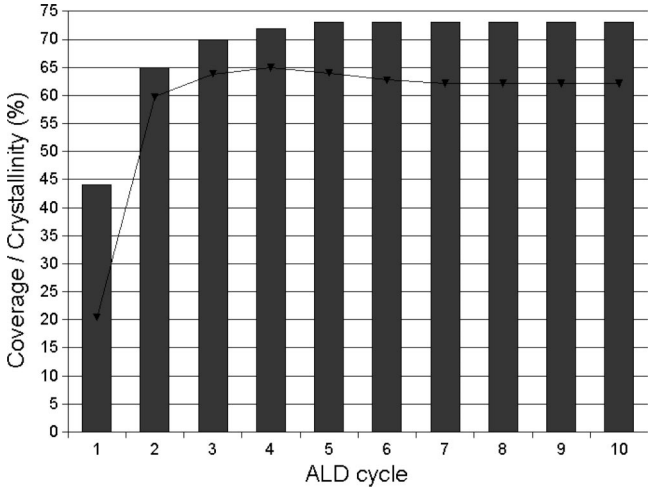

Figure 11. Evolution of coverage rates (HfO_2 coverage) and crystallinity with respect to ALD cycles number. The coverage is cumulative. The legend is the same as in Figure 10.

an electronvolt. This suggests that the calibration of a mechanism, or a class of mechanisms, is accessible through KMC by confrontation to experiment.

Waiting for subsequent quantum contributions or experiment investigations, we adopt this single value of 1.5 eV as a first approximation for all the densification mechanisms. We hope that it may help and shall be used as a basis for DFT investigations, which can now allow us to distinguish between different types of densification mechanisms (listed in Table 1), associated with different activation barriers, and to determine the most efficient ones. This proves that the simulator can lend itself to a calibration on experimental data, even in a very approximate way but still necessary to get insights toward complex physicochemical issues.

3.2.4. Kinetics of Growth. Until now, we have validated the basics of the method and the first mechanisms introduced in the KMC scheme, without exceeding the first phase of the first ALD cycle. We now will try to go beyond this stage by carrying out simulations on several ALD cycles under standard conditions: at 300 °C and 1.33 mbar pressure for the two precursors. The phases of injection will last 50 ms, as in experiments, and are followed by a 4 s of purge.

In experiments, several modes of growth are successively observed.[70,71] After the first cycle, consuming a great number of metal precursors, a slow transient state is established to complete the coverage of the substrate. Then, a steady operation starts, faster, where HfO_2 is deposited on HfO_2 substrate. By using atomic scale KMC, we try to reproduce all these aspects of the kinetics of growth on (10×10) and (20×20) atoms substrates during tens of ALD cycles.

We first launched a simulation of 10 ALD cycles, whereas the mechanism of opening of a siloxane bridge was not yet implemented in the software package. Indeed, it was experimentally observed that that the opening of siloxane bridges only took place at higher temperatures.

Figure 11 shows the evolution of the cumulated coverage (HfO_2 coverage) and the total crystallinity. We note a great number of incorporations during the first cycle leading to 44% coverage. This value is slightly larger than experimental observations (35%), undoubtedly because of an overevaluation of the hydroxyl concentrations given by the Zhuravlev model[72] Then, from cycle 2 to 5, the coverage saturates gradually until a maximum of 73% is reached. Beyond cycle 5, the growth is stopped. This is caused by the inability of the densification mechanisms to be fully efficient. An examination of the final structure indicates specific sites where further densification mechanisms should occur but cannot be performed by the mechanisms already implemented in our software package. We are currently considering rewriting the algorithm used to treat densification mechanisms to overcome this problem. The rate of crystallinity follows the same tendency and is stabilized around 62%, meaning that the densification had taken place, but not fully, because of, at least, an unsatisfactory description of densification. However, one cannot be satisfied with this situation because the experiments show that the growth continues, certainly slowly, after the strong coverage observed after the first cycle.[70,71] An opening of the siloxane bridges by a water molecule has been suggested that could allow the total coverage to be reached. The opening of the siloxane bridges is postponed during the hydrolysis phases and could bring additional reactive sites on the initial surface. However, no consensus exists to explain how the HfO_2 coverage is reached exactly. Currently, effort is undertaken on this subject through the improvement of the densification mechanisms suggested recently by DFT investigations.[73]

4. Conclusions

This work presents an original kinetic Monte Carlo algorithm, developed within a multiscale strategy: from molecule−surface interactions treated mostly at the DFT level of modeling, to atomic scale film growth performed via a KMC technique. We have given details on how ab initio calculations can help in the identification of the relevant elementary reaction mechanisms, before their definite implementation into the Monte Carlo simulator that can handle millions of atoms during seconds of simulation runs. We then show how to develop a KMC method aimed at dealing with a promising experimental deposition procedure: the ALD. This technique is expected to result in a unique change in microelectronics history by replacing traditional Si/SiO_2 interface by a deposited high-k material onto silicon. The basics of a specific KMC have been reported, and preliminary examples for the validation of the overall multiscale strategy are detailed. We have shown how KMC provides a unique and fundamental understanding of the growth mechanism and growth kinetics of the dielectric (HfO_2) onto silicon. The relation of KMC with experiment is lighted. We have also shown that KMC, allowing a global view of mesoscopic structures, may shed light on shortcomings in the model. New mechanisms can then be considered for ab initio DFT investigations. The relevant example here has been the case of densification mechanisms. We hope that this work will bring new advances for better control of the $HfO_2/SiO_2/Si$ systems and for further optimization of the processing parameters with the aim of integrating hafnium oxide in the heart of future generations of MOS device. Beyond this targeted application, we believe that the development of the

KMC, detailed here, is generic and may serve other new concepts in nano- and bionanotechnologies.

Acknowledgment. C.M. acknowledges the "Conseil regional de la Martinique" for the funding.

Appendix

A. **Temporal Dynamics.** Kinetic Monte Carlo approaches differ from static Monte Carlo techniques by the introduction of time. Most of the Monte Carlo procedures used in condensed matter physics are static (the Metropolis algorithm for instance), and their interest concerns the equilibrium structure properties. KMC is totally different in philosophy. Here, the Monte Carlo technique is introduced for the stochastic aspects, in connection with the time incremental procedure, that is, it is not always the most probable event that occurs. Different algorithms do exist for KMC. We suggest in the following a procedure that becomes efficient, with regard of the more conventional BKL algorithm, when dealing with many different events related to the same mechanism, but having different probabilities. This means that the probability depends also on the site of occurrence. This is the case of systems where local deformation energy is taken into account (each event has therefore a different probability of occurrence) and where the system exhibits a complex chemistry.

A1. **Atomic Layer Deposition (ALD).** The KMC software discussed here is built to simulate the ALD experimental process. ALD consists of four phases: precursor pulse, precursor purge, hydrolysis, and water purge. Each one has its own thermodynamic parameters and duration.. Some mechanisms are always possible, whereas others can only occur in a typical phase. For instance, "precursor arrival" will obviously exist during the first phase only. Furthermore, the complete ALD process consists of several cycles of these four phases.

A2. **Time Management.** When the software is launched, after preliminary initializations (parameters, mechanisms, neighborhood, configuration), it makes a global scan to determine which events are authorized and which are forbidden. Authorized ones get a "specific occurrence time": this is the time that the considered event typically takes to occur as soon as it becomes authorized. Forbidden ones get the maximum time so that they can never occur.

The "specific occurrence time" of the event m on site (i, j, k) is given by

$$T_{i,j,k,m} = \frac{-\log(Z)}{\lambda_m}$$

where Z is a random number uniformly distributed between 0 and 1 and λ_m is the probability, per unit time, of occurrence of the mechanism. It is expressed as

$$\lambda_m = \nu \exp\left(\frac{\Delta E_m}{k_B T}\right)$$

where ν is on the order of the typical lattice vibration frequency, $\Delta E_m$is the activation energy of the mechanism, k_B the Boltzmann constant, and T the temperature. The two arrival mechanisms (1 precursor arrival and 2 water arrival) obey Maxwell−Boltzmann statistics of the gas phase and have different probability expressions

$$\lambda_{1,2} = \frac{\mathrm{Cst}PS}{\sqrt{M_{1,2}T}}$$

where Cst is a constant, P the pressure, S the elementary 2D-cell area, $M_{1,2}$ the molar mass of the considered species, and T the temperature. In this scheme, we have a huge list of "specific times", a kind of "calendar", just as if all events that will occur were already foreseen. Not exactly in fact, because this calendar will often be updated as the configuration evolves. As soon as the calendar is updated, the software finds the minimum "specific occurrence time" and the corresponding event occurs. After this minimum time has passed, it is withdrawn from the other times contained in the "calendar". Then, the configuration is edited and the pertinent events (that are likely to become authorized) are filtered. We then go back to the first KMC stage where the minimum time is searched.

References

(1) Packan, P. A. *Science.* **1999**, *285*, 2079.

(2) Wilk, G. D.; Wallace, R. M.; Anthony, J. M. *J. Appl. Phys.* **2001**, *89*, 5243.

(3) Wilk, G. D.; Muller, D. A. *Appl. Phys. Lett* **2003**, *83*, 3984.

(4) (a) George, S. M.; OTT, A. W.; Klaus, J. W. *J. Phys. Chem.* **1996**, *100*, 13121. (b) Xu, Z.; Houssa, M.; Gendt, S. D.; Heyns, M. *Appl. Phys. Lett.* **2002**, *80*, 1975.

(5) Ferrari, S.; Scarel, G.; Wiemer, C.; Fanciulli, M. *J. Appl. Phys.* **2002**, *92*, 7675.

(6) Park, H. B.; Cho, M. J.; Park, J.; Lee, S. W.; Hwang, C. S.; Kim, J. P.; Lee, J. H.; Lee, N. I.; Kang, H. K.; Lee, J. C.; Oh, S. J. *J. Appl. Phys.* **2003**, *94*, 3641.

(7) Kawahara, T.; Torii, K. *IEICE Trans. Elect.* **2004**, *E87C* (1), 2–8.

(8) Ganem, J. J.; Trimaille, I.; Vickridge, I. C.; Blin, D.; Martin, F. *Nucl. Instrum. Methods Phys. Res., Sect. B* **2004**, *219*, 856.

(9) Green, M. L.; Ho, M. Y.; Busch, B.; Wilk, G. D.; Sorsch, T.; Conard, T.; Brijs, B.; Vandervorst, W.; Raisanen, P. I.; Muller, D.; Bude, M.; Grazul, J. *J. Appl. Phys.* **2002**, *92*, 7168.

(10) Triyoso, D. H.; Hegde, R. I.; Grant, J.; Fejes, P.; Liu, R.; Roan, D.; Ramon, M.; Werho, D.; Rai, R.; La, L. B.; Baker, J.; Garza, C.; Guenther, T.; White, B. E.; Tobin, P. J. *J Vac. Sci. Technol. B.* **2003**, *22*, 2121.

(11) Rittersma, Z. M.; Roozeboom, F.; Verheijen, M. A.; van Berkum, J. G. M.; Dao, T.; Snijders, J. H. M.; Vainonen-Ahlgren, E.; Tois, E.; Tuominen, M.; Haukka, S. *J. Electrochem. Soc.* **2004**, *151*, 716.

(12) Chang, H. S.; Hwang, H.; Cho, M. H.; Moon, D. W. *Appl. Phys. Let.* **2005**, *86*, 031906.

(13) Triyoso, D. H.; Ramon, M.; Hegde, R. I.; Roan, D.; Garcia, R.; Baker, J.; Wang, X. D.; Fejes, P.; White, B. E.; Tobin, P. J. *J. Electrochem. Soc.* **2005**, *152*, 203.

(14) Cho, M.; Park, H. B.; Park, J.; Lee, S. W.; Hwang, C. S.; Jeong, J.; Kang, H. S.; Kim, Y. W. *J. Electrochem. Soc.* **2005**, *152*, F49.

(15) Kukli, K.; Aaltonen, T.; Aarik, J.; Lu, J.; Ritala, M.; Ferrari,

S.; Harsta, A.; Leskela, M. *J. Electrochem. Soc.* **2005**, *152*, F75.

(16) Triyoso, D. H.; Hegde, R. I.; White, B. E.; Tobin, P. J. *J. Appl. Phys.* **2005**, *97*, 124107.

(17) Hellin, D.; Delabie, A.; Puurunen, R. L.; Beaven, P.; Conard, T.; Brijs, B.; De Gendt, S.; Vinckier, C. *Anal. Sci.* **2005**, *21*, 845.

(18) Kirsch, P. D.; Quevedo-Lopez; MA; Li, H. J.; Senzaki, Y.; Peterson, J. J.; Song, S. C.; Krishnan, S. A.; Moumen, N.; Barnett, J.; Bersuker, G.; Hung, P. Y.; Lee, B. H.; Lafford, T.; Wang, Q.; Gay, D.; Ekerdt, J. G. *J. Appl. Phys.* **2006**, *99*, 023508.

(19) Park, I. S.; Lee, T.; Choi, D. K.; Ahn, J. *J. Korean Phys. Soc.* **2006**, *49*, S544.

(20) Cho, M. J.; Degraeve, R.; Pourtois, G.; Delabie, A.; Ragnarsson, L. A.; Kauerauf, T.; Groeseneken, G.; De Gendt, S.; Heyns, M.; Hwang, C. S. *IEEE Trans. Electron Devices* **2007**, *54*, 752.

(21) Nyns, L.; Hall, L.; Conard, T.; Delabie, A.; Deweerd, W.; Heyns, M.; Van Elshocht, S.; Van Hoornick, N.; Vinckier, C.; De Gendt, S. *J. Electrochem. Soc.* **2006**, *153*, F205.

(22) Ritala, M.; Leskela, M.; Niinisto, L.; Prohaska, T.; Friedbacher, G.; Grasserbauer, M. *Thin Solid Films* **1994**, *250*, 72.

(23) Aarik, J.; Aidla, A.; Kiisler, A. A.; Uustare, T.; Sammelselg, V. *Thin. Solid Films* **1999**, *340*, 110.

(24) Kukli, K.; Ihanus, J.; Ritala, M.; Leskela, M. *Appl. Phys. Lett.* **1996**, *68*, 3737.

(25) Aarik, J.; Aidla, A.; Kiisler, A. A.; et al. *Thin Solid Films* **1999**, *340*, 110.

(26) Aarik, J.; Aidla, A.; Mandar, H. *J. Cryst. Growth* **2000**, *220*, 105.

(27) Aarik, J.; Aidla, A.; Kikas, A. *Appl. Surf. Sci.* **2004**, *230*, 292.

(28) Kukli, K.; Aarik, J.; Uustare, T. *Thin Solid Films* **2005**, *479*, 1.

(29) de Almeida, R. M. C.; Baumvol, I. J. R. *Surf. Sci. Rep.* **2003**, *49*, 1.

(30) Wallace, R. M.; Wilk, G. D. *Crit. Rev. Solid State Mater. Sci.* **2003**, *28*, 231.

(31) Wang, D.; Wang, Q.; Javey, A. *Appl. Phys. Lett.* **2003**, *83*, 2432.

(32) Wong, H.; Iwai, H. *Microelectron. Eng.* **2006**, *83*, 1867.

(33) Aarik, J.; Aidla, A.; Sammelselg, V.; Siimon, H.; Uustare, T. *J. Cryst. Growth* **1996**, *169*, 496.

(34) Puurunen, R. L. *Chem. Vap. Deposition.* **2005**, *11*, 79.

(35) Heyman, A.; Musgrave, C. B. *J. Phys. Chem. B.* **2004**, *108*, 5718.

(36) Samantaray, C. B.; Sim, H.; Hwang, H. *Appl. Surf. Sci.* **2005**, *242*, 121.

(37) Elliott, S. D.; Pinto, H. P. *J. Electroceram.* **2004**, *13*, 117.

(38) Samantaray, C. B.; Sim, H.; Hwang, H. *Appl. Surf. Sci.* **2004**, *239*, 101.

(39) Mukhopadhyay, A. B.; Musgrave, C. B. *App. Phys. Lett.* **2007**, *90*, 173120.

(40) Forst, C. J.; Blochl, P. E.; Schwarz, K. *Comput. Mater. Sci.* **2003**, *27*, 70.

(41) Kawamoto, A.; Cho, K. J.; Dutton, R. *J. Comput.-Aided Mater. Des.* **2001**, *8*, 39.

(42) Musgrave, C. B.; Han, J. H.; Gordon, R. G. *Abstr. Pap. Am. Chem. Soc.* **2003**, *226*, U386.

(43) Mukhopadhyay, A. B.; Sanz, J. F.; Musgrave, C. B.; Han, J. H.; Gordon, R. G. *J. Phys. Chem. C.* **2007**, *26*, 9203.

(44) Ganem, J. J.; Trimaille, I.; Vickridge, I. C.; Blin, D.; Martin, F. *Nucl. Instrum. Methods Phys. Res., Sect. B* **2004**, *219*, 856.

(45) Mui, C.; Musgrave, C. B. *J. Phys Chem. B.* **2004**, *108*, 15150.

(46) Xu, Y.; Musgrave, C. B. *Appl. Phys. Lett.* **2005**, *86*, 192110.

(47) Mukhopadhyay, A. B.; Musgrave, C. B. *Chem. Phys. Lett.* **2006**, *421*, 215.

(48) Ren, J.; Zhang, Y. T.; Zhang, D. W. *THEOCHEM* **2007**, *803*, 23.

(49) Jeloaica, L.; Esteve, A.; Djafari Rouhani, M.; Esteve, D. *Appl. Phys. Lett.* **2003**, *83*, 542.

(50) Esteve, A.; Jeloiaca, L.; Mazaleyrat, G.; Dkhissi, A.; Djafari Rouhani, M.; Ali Messaoud, S.; Fazouan, N. *MRS Bull.* **2003**, *786*, 35.

(51) Jeloaica, L.; Esteve, A.; Dkhissi, A.; Djafari Rouhani, M. *Comput. Mater. Sci.* **2005**, *33*, 2005.

(52) Becke, A. D. *J. Chem. Phys.* **1993**, *98*, 5648.

(53) Lee, C.; Yang, W.; Parr, R. G. *Phys. Rev. B* **1988**, *37*, 785.

(54) Bergner, A.; Dolg, M.; Kuechle, W.; Stoll, H.; Preuss, H. *Mol. Phys.* **1993**, *80*, 1431.

(55) Schaefer, A.; Horn, H.; Ahlrichs, R. *J. Chem. Phys.* **1992**, *97*, 2571.

(56) Schaefer, A.; Huber, C. F.; Ahlrichs, R. *J. Chem. Phys.* **1994**, *100*, 5829.

(57) Weldon, M.; Stefanov, B. B.; Raghavachari, K.; Chabal, Y. I. *Phys. Rev. Lett.* **1997**, *79*, 2851.

(58) Helgaker, T. *Chem. Phys. Lett.* **1991**, *182*, 503.

(59) (a) Ahlrichs, R.; Bär, M.; Häser, M.; Horn, H.; Kölmel, C. *Chem. Phys. Lett.* **1989**, *162*, 165. (b) Schäfer, A.; Horn, H.; Ahlrichs, R. *J. Chem. Phys.* **1992**, *97*, 2571. (c) Schäfer, A.; Huber, C.; Ahlrichs, R. *J. Chem. Phys.* **1994**, *100*, 5829.

(60) Frisch, M. J.; Trucks, G. W.; Schlegel, H. B.; Scuseria, G. E.; Robb, M. A.; Cheeseman, J. R.; Zakrzewski, V. G.; Montgomery, J. A.; Stratmann, R. E.; Burant, J.; Dapprich, S.; Millam, J. M.; Daniels, A. D.; Kudin, K. N.; Strain, M. C.; Farkas, O.; Tomasi, J.; Barone, V.; Cossi, M.; Cammi, R.; Mennucci, B.; Pomelli, C.; Adamo, C.; Clifford, S.; Ochterski, J.; Petersson, G. A.; Ayala, P. Y.; Cui, Q.; Morokuma, K.; Salvador, P.; Dannenberg, J. J.; Malick, D. K.; Rabuck, A. D.; Raghavachari, K.; Foresman, J. B.; Cioslowski, J.; Ortiz, J. V. B., A. G.; Stefanov, B. B.; Liu, G.; Liashenko, A.; Piskorz, P.; Komaromi, I.; Gomperts, R.; Martin, R. L.; Fox, D. J.; Keith, T.; Al-Laham, M. A.; Peng, C. Y.; Nanayakkara, A.; Challacombe, M.; Gill, P. M. W.; Johnson, B. G.; Chen, W.; Wong, M. W.; Andres, J. L.; Gonzalez, C.; Head-Gordon, M.; Replogle, E. S.; Pople, J. A.; *Gaussian 03*, revision D.02; Gaussian,Inc.: Wallingford CT, 2004.

(61) Kotrla, M. *Comput. Phys. Commun.* **1996**, *97*, 82.

(62) Smilauer, P.; Vvedensky, D. D. *Phys. Rev. B.* **1995**, *52*, 14263.

(63) Schofield, W. C. E.; McGettrick, J. D.; Badyal, J. P. S. *J. Phys. Chem.B.* **2006**, *110*, 17161.

(64) Wyckoff, R., Ed. *Crystal Structure*; John Wiley & Sons: New York, 1965; Vol. 1, p 231.

(65) Ritala, M.; Leskela, N. in *Handbook of Thin Film Materials*; Nalwa, H. S., Ed.; Academic Press: New York, 2001; Vol. 1, p 57.

(66) Rahtu, A.; Ritala, M. *J. Mater. Chem.* **2002**, *12*, 1484.

(67) Widjaja, Y.; Musgrave, C. B. *J. Chem. Phys.* **2002**, *117*, 1931.

(68) Widjaja, Y.; Musgrave, C. B. *Appl. Phys. Lett.* **2002**, *81*, 304.

(69) Han, J. H.; Gao, G.; Widjaja, Y.; Garfunkel, E.; Musgrave, C. B. *Surf. Sci.* **2004**, *550*, 199.

(70) Blin, D. PhD thesis, University of Montpellier, 2003.

(71) Renault, O.; Samour, D.; Rouchon, D.; Holliger, Ph.; Papon, A. M.; Blin, D.; Marthon, S. *Thin Solid Films* **2003**, *428*, 190.

(72) Zuravlov, L. T. *Colloids Surf. A* **2000**, *173*, 1.

(73) Olivier, S.; Ducere, J. M.; Mastail, C.; Esteve, A.; Landa, G.; Djafari Rouhani, M. *Chem. Mater.* **2008**, *20*, 1555.

CT8001249